Journal of Asian Ceramic Societies

ISSN: (Print) (Online) Journal homepage: https://www.tandfonline.com/loi/tace20

Pulse electro co-deposition of submicron-sized TiC reinforced Ni–W coatings: tribological and corrosion properties

Serhat Dilek, Hasan Algül, Abdülkadir Akyol, Ahmet Alp, Hatem Akbulut & Mehmet Uysal

To cite this article: Serhat Dilek, Hasan Algül, Abdülkadir Akyol, Ahmet Alp, Hatem Akbulut & Mehmet Uysal (2021) Pulse electro co-deposition of submicron-sized TiC reinforced Ni–W coatings: tribological and corrosion properties, Journal of Asian Ceramic Societies, 9:2, 673-685, DOI: 10.1080/21870764.2021.1911058

To link to this article: https://doi.org/10.1080/21870764.2021.1911058

Published online: 12 Apr 2021.

JOURNAL OF ASIAN CERAMIC SOCIETIES
2021, VOL. 9, NO. 2, 673–685
https://doi.org/10.1080/21870764.2021.1911058

THE CERAMIC SOCIETY OF JAPAN
THE KOREAN CERAMIC SOCIETY
Taylor & Francis
Taylor & Francis Group

FULL LENGTH ARTICLE

Pulse electro co-deposition of submicron-sized TiC reinforced Ni–W coatings: tribological and corrosion properties

Serhat Dilek[a], Hasan Algül[a], Abdülkadir Akyol[a], Ahmet Alp[a], Hatem Akbulut[a,b,c] and Mehmet Uysal[a,b]

[a]Sakarya University, Faculty of Engineering, Department of Metallurgy and Materials Engineering, Sakarya, Turkey; [b]Sakarya University, Sakarya University Research and Development Center (SARGEM), Esentepe Campus, Sakarya, Turkey; [c]NESSTEC Energy & Surface Technologies A.S., Technology Development Zones, Sakarya, Turkey

ABSTRACT

Nickel–Tungsten–Titanium carbide (Ni–W–TiC) coatings were produced by pulse electrodeposition from a Ni–W electrolyte containing TiC particles. The effects of TiC concentration in the electrolyte on the morphology, crystallite size, microstrain, mechanical, tribology and electrochemical properties of TiC reinforced Ni–W co-depositions were investigated. The highest hardness of 8.3 GPa and modulus of elasticity of 207 GPa were observed in the case of the coating produced at 15 g/L TiC concentration in the electrolyte. The increase in the H/E and H^3/E^2 ratios led to displaying excellent wear resistance of the Ni–W–TiC co-depositions besides high resistance to plastic deformation. A direct correlation was observed between nanoindentation and wear resistance results of reinforced TiC co-depositions. It has also been shown by electrochemical impedance spectroscopy and potentiodynamic polarization analysis that TiC particles can improve the electrochemical properties of the co-depositions because of their barrier effect.

ARTICLE HISTORY
Received 30 October 2020
Accepted 27 March 2021

KEYWORDS
Electro co-deposition; composite coating; nanoindentation; H/E ratio; tribology

1. Introduction

Electrodeposition is a well-known method for the production of high-performance metal or alloy coatings and this technique has been extensive used for protecting surfaces from friction and environmental degradation [1–3]. Chrome plating is the most common type of electrodeposition, with its high hardness, excellent corrosion, wear resistance and low friction coefficient. Conventionally, chrome coatings are generally performed in coating baths containing Cr^{+6} ions. The presence of Cr^{+6} ions in the electrolyte poses a great danger to human health and the environment, which limits this coating process [4–6]. Many studies have been focusing on replacing chrome plating, to improve the wear, mechanical and electrochemical properties [7–9].

Electro co-deposition of nickel-–based (Ni–W, Ni–Mo, Ni–Cr, etc.) is one of the few surfaces finishing processes using a wide variety of industrial applications utilized to enhance the properties such as hardness, wear resistance and corrosion resistance. Nickel-based composite coatings not only enhance the appearance of materials but also improve materials performance that can be an alternative to environmentally hazardous functional chromium coatings [10,11]. Among them, Ni–W alloy deposition had been regarded as appropriate to replace the hard chromium coating due to their high wear resistance, excellent mechanical property and corrosion resistance [12,13]. Ni–W alloy coatings have found several applications fields such as engine valves, piston rings, electrical connectors, molding dies, internal combustion engines, etc. due to their high corrosion and wear resistance and thermal stability. Different researchers report that the hardness of the Ni–W coating has to change between 460 and 670 Hv depending on the crystallite size and W content of coating [14]. The Ni–W alloy (1.4 wt% tungsten) showed a tensile strength of about 1.3 GPa and tensile ductility of 2.7% [15]. It was found that the Ni–W alloy displayed a tensile strength of ~2300 MPa and good ductility. Electroplated Ni–W alloys were reported to display varied toughness between 5.1 and 8.9 MPa√m at 21 wt% W composition depending on the heat treatment [16]. To further enhance the tribological and electrochemical properties of Ni–W alloy, various types of particle reinforcements, such as SiC, PTFE, Al_2O_3, BN, Si_3N_4, and have been incorporated in the alloy matrix [17–20]. Sangeetha et al. [21] investigated effect of BN particles on the corrosion resistance of the Ni–W–BN coating and noticed that with an increase in the concentration of BN particles in the electrolyte, the corrosion resistance of Ni–W–BN co-deposition improved. He et al. [22] produced Ni–W–MWCNT coatings by pulse electrodeposition and reported that the corrosion resistance was improved after incorporation of MWCNT. Gyawali et al. reported [23] that Ni–W–Si_3N_4 coatings produced by electrodeposition and optimum content of the particles

CONTACT Mehmet Uysal mehmetu@sakarya.edu.tr NESSTEC Energy & Surface Technologies A.S., Technology Development Zones, Sakarya, Turkey.

in the matrix results in coating with better hardness and elastic modulus. Li et al. [24] reported Ni–W/SiC coatings produced by pulse electrodeposition and found that the concentration of ceramic particles in the electrolyte significantly affects the wear performance. Yi et al. [25] demonstrated that the Ni–W–SiO_2 co-deposition displays high corrosion resistance and low friction coefficient compared with the Ni–W alloy. Beltowska et al. [19] produced Ni–W–ZrO_2 coating through pulse electrodeposition and results that ZrO_2 particles can significantly improve the hardness and tribological properties of the Ni–W matrix. Goldasteh et al. [26] investigated the effect of ceramic particles on the microhardness and corrosion resistance of Ni–W–TiO_2 coatings deposited by the pulse electrodeposition method and the results found the incorporation of TiO_2 particles caused enhancement of both wear and corrosion resistance of coatings in 0.5 M NaCl solution.

Titanium carbide (TiC) possesses a high melting temperature (3150°C), high hardness superior, good corrosion and wear resistance [27]. Moreover, the TiC reinforced co-deposition has more excellent wear, hardness and corrosion performance. Li et al. [28] have examined the electrochemical properties of the Ni–B–TiC coatings produced by pulsed electrodeposition process and found that the corrosion resistance of Ni–B matrix improved with increasing particle concentration in the bath. Choi et al. [29] produced Ni–W–TiC coating by electrodeposition and found that TiC particles can significantly increase the wear resistance of coatings. Therefore, TiC is used as reinforcement to improve the tribological, mechanical, and electrochemical resistance for various applications. The study concerning TiC reinforced Ni-based alloy coating is scarce and only a few researchers have investigated the effect of the ceramic particle on wear properties of TiC reinforced Ni–W alloy coatings.

To the best of our knowledge, no article has been published on the morphology, nanomechanical, tribology and electrochemical properties of Ni–W–TiC co-deposition produced using pulse electrodeposition. The microstructure and morphology of the produced samples were also characterized. The mechanical properties of the TiC co-deposition obtained with different TiC concentrations were carried out with nanoindentation. Moreover, the microstrain of the coating was calculated after the addition of ceramic particles into the matrix. The wear performance of coating was investigated in detail. The electrochemical properties were evaluated using polarization curve and electrochemical impedance spectroscopy techniques.

2. Experimental process

Ni–W and Ni–W–TiC coatings were deposited on the substrate from an electrolyte containing Ni(II), W(VI) ions and TiC submicron particles suspended in the electrolyte with the particle size distribution between 0.1 and 0.5 μm by pulse electrodeposition method. The composition of the electrolyte solution used and operational parameters are listed in Table 1. The mild steels used as substrate were polished by 600, 800 and 1200 emery papers for obtaining a smooth surface, to eliminate the passive oxide layer and contaminations. After that, the substrates were activated with 1 M sulfuric acid solution for 30 s and washed with distilled water then immediately placed into the bath. Before the electrodeposition process, in order to obtain a uniform dispersion of the ceramic particles, the plating solution is ultrasonically agitated at a power of 100 W for 1 h subsequent by magnetically stirring at a stirring rate of 250 rpm. Cetyltrimethyl ammonium bromide (CTAB) as surfactant used for particle dispersion to avoid agglomeration of TiC in a plating bath. The plating bath temperature and pH values were maintained at 75°C and ~8.5, respectively. Pure nickel plate and steel substrate with an area of 5×5 cm^2 were used as anode and cathode, respectively and the nickel anode was positioned 15 mm away from the cathode. For comparison, unreinforced Ni–W alloy was deposited without particles in the plating bath under the same conditions.

Cross-sectional and surface morphologies of the samples were investigated with a field emission scanning electron microscope. Energy Dispersive X-ray Spectroscopy (EDAX) attached with FESEM (JEOL JSM 6060 LV)) was used to determine the composition of samples. Phase analysis of the co-deposition was performed using X-ray diffraction (Rigaku D/max–2400) at a speed of 1°/min in the 2θ range of 20–90 with Cu Kα radiation source. According to the FWHM of all peaks of the samples, the crystallite size and microstrain (ε) of samples have been calculated according to the Williamson–Hall equation [30].

Nano hardness and elastic modulus of the Ni–W alloy and Ni–W–TiC coatings deposited with various TiC concentrations were measured using the nanoindentation technique (Anton Paar Nanoindentation tester: NHT3) with a standard diamond Berkovich tip from cross-sections of the polished samples. Nanoindentation tests were carried out at a maximum load of 100 mN and a loading rate of 20 mN/s for 30 s and then unloaded completely. After loading–unloading indentation tests, hardness and elastic modulus were calculated from the load vs.

Table 1. Composition of bath and deposition parameters.

$NiSO_4 \cdot 7H_2O$ (g/L)	16	pH	8.5
$Na_2WO_4 \cdot 2H_2O$ (g/L)	46	Temperature (°C)	75
$Na_3C_6H_5O_7 \cdot 2H_2O$ (g/L)	147	Time (min)	45
NH_4Cl (g/L)	25	Current density A/dm^2	10
NaBr (g/L)	16	t_{on}–t_{off} (ms)	50–50
TiC concentration (g/L)	5–15–30		
CTAB (g/L)	0.2		

depth curve in terms of the Oliver and Pharr method [31].

The reciprocating ball-on-disc tests (CSM Instruments Tribometer – Switzerland) were carried out to determine the tribological properties of the depositions. An M50 steel ball with a diameter of 10 mm which suitable to DIN 50 324 and ASTM G 99–95a (Ø 10 mm) was used as the counter body. All tests were performed under a 1 N load with a sliding speed of 100 mm/s under dry sliding conditions. The worn surfaces of the samples were evaluated by SEM. To calculate the area of worn material after the wear test, wear tracks were measured by using a surface profilometer (KLA Tencor P6), and subsequently, the wear rates were calculated as shown in Equation (1) [32]:

$$\text{Wearrate} = V/FXS, \quad (1)$$

where: V is volume loss of sample, F is load and S is sliding distance.

Electrochemical measurements of samples were performed using potentiodynamic polarization technique and electrochemical impedance spectroscopy (EIS) using a Gamry Interface 1000 potentiostat in a conventional three-electrode cell with a 3.5 wt% NaCl solution. The electrochemical cell set-up consisted of a surface area of 1 cm^2 and was used as working electrodes, platinum foil as a counter electrode and saturated calomel electrode as the reference electrode. Before the measurements, the open circuit potential (OCP) of the coatings was recorded for 1 h. The potentiodynamic polarization measurements were performed to utilize the corrosion properties of samples under a potential range from −100 mV to +100 mV. EIS measurements were close to open circuit potential with an amplitude of 10 mV and frequency ranging from 0.01 to 100 000 Hz.

3. Results and discussion

The surface morphologies of unreinforced Ni–W coating and Ni–W–TiC co-depositions fabricated at various ceramic particle concentrations by pulse electrodeposition are shown in Figure 1. As shown in Figure 1a, the unreinforced Ni–W coating surface is smooth and there seems a dense structure has been provided. Moreover, Ni–W coating shows a mixture of polyhedrons and needle-shaped grains. The incorporation of ceramic particles into the matrix has a great effect on the surface morphologies of the Ni–W coatings. It is obvious that the surface of Ni–W–TiC coating deposited with 5 g/L has a rougher structure than the unreinforced Ni–W alloy coating due to high nucleation sites providing polycrystalline grain growth and therefore preventing columnar growth as can be seen from Figure 1b–1d. Also, the inhomogeneous growth and grain formation on the surface of the coatings, which may be due to the preferential deposition of nickel on the TiC particle surfaces when these were embedded on the substrate instead of Ni atoms depositing uniformly on the steel [33]. As shown in Figure 1c, the morphology of the Ni–W–TiC co-deposition prepared with TiC concentrations of 15 g/L yielded smoother surfaces with the growth of smaller crystals and revealed denser structures when

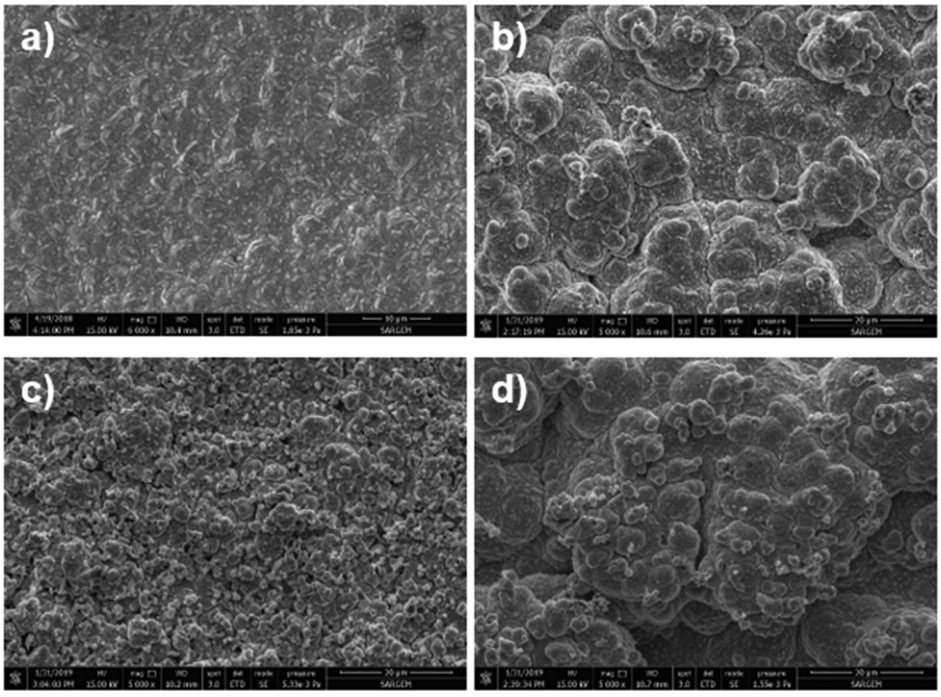

Figure 1. FESEM surface micrographs of coatings produced by the pulse electrodeposition with TiC concentrations of (a) 0 g/L, (b) 5 g/L, (c) 15 g/L and (d) 30 g/L.

compared with other coatings. This effect can be understood by appreciating that the incorporated ceramic particles could be the sites for the nucleation of nickel growth and at higher TiC particle concentrations led to more nucleation sites on the nickel matrix and the roughness was reduced. This is because experimental investigation has shown that the amount of co-deposited TiC particles was highest in the case of 15 g/L TiC concentrations in the electrolyte. An increasing amount of TiC particles is believed to cause higher nucleation sites thus increasing the heterogeneous nucleation and growth [34]. Because of this effect, the amount of suspended particles in the electrolyte is fairly low in the 5 g/L TiC particle added electrolyte condition (Figure 1b) and for the 30 g/L TiC concentration in the electrolyte, the deposited Ni matrix grains seems to be coarser. Segregation of TiC particles in the electrolyte most probably from the insufficient amount of surfactant material or low electrolyte stirring rate for this concentration revealed rough deposited surfaces for the Ni–W–TiC co-deposited composite.

Figure 2 shows SEM images of cross-sections of Ni–W and Ni–W–TiC coatings deposited with various TiC concentrations. It can be seen that there is good adhesion between the substrate and coatings for all samples, where no discontinuity is observed between them. Moreover, there are no cracks, porosity on the cross-section of all coatings. Also, it can be seen that the thickness of all samples measured to be between ~28 and 35 µm with a slight thickness increment with increasing particle concentration in the electrolyte. This reason for different coating thickness may be due to the deposition rate of nickel ions. The unreinforced Ni–W alloy coating shows a smooth surface with a thickness of about ~25 µm. As is seen from Figure 2b–c, the TiC ceramic particles are well distributed in the cross-section of the deposited coatings. The reason for the increase in the content of incorporated TiC particles with increasing TiC concentration in the plating bath can be attributed to Guglielmi's model [35,36], in which the co-deposition of TiC depends on two absorption models which of physical adsorption and strong adsorption. The physical absorption step consists of particle concentration in the solution. In the second step dominated by a high overpotential, the rate of adsorption of co-deposited particles is high. Ni–W–TiC (15 g/L) coating was characterized by EDX spectroscopy for investigating the elemental composition and distribution of particles. As shown in Figure 3, TiC particles were uniformly distributed in the Ni(W) matrix without apparent agglomeration and the TiC particles were well bonded onto the surface of the coating. Figure 4 shows the amount of the tungsten and TiC ceramic particles in the coatings versus the concentration of the TiC particles at the plating bath. The main reason for the decrease in the amount of tungsten coated with Ni by increasing TiC particle concentration is that Ni ions absorb much more actively on TiC particles than tungsten ions [37]. The graph clearly shows that the amount of TiC ceramic particles incorporated in the Ni(W) matrix increases with an increase in TiC ceramic particle concentration. However, as stated above, increasing the ceramic particle concentration beyond 15 g/L resulted in

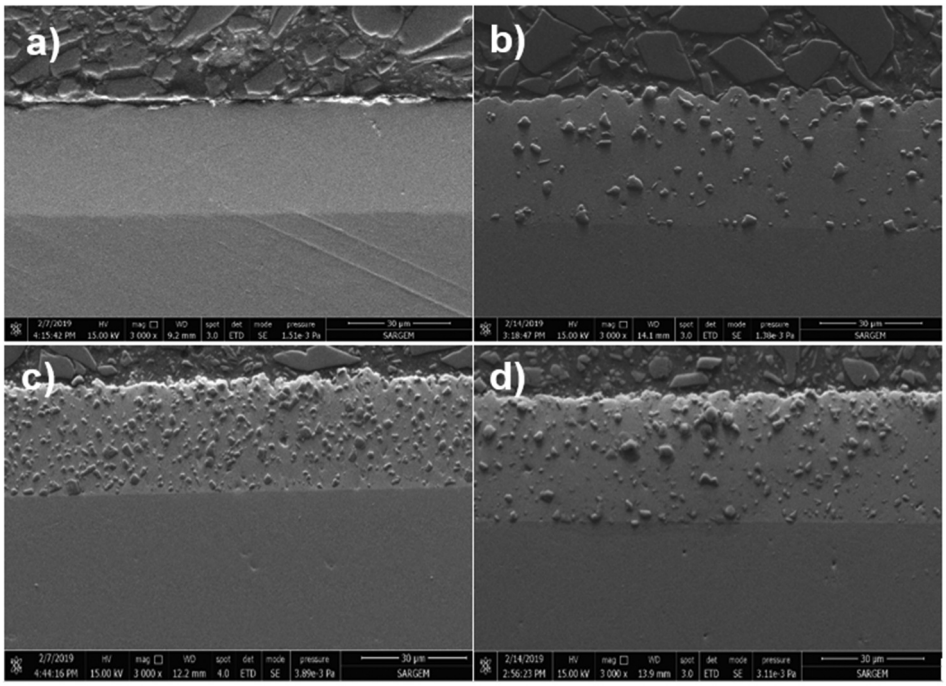

Figure 2. The cross-sectional SEM images for unreinforced Ni–W and Ni–W–TiC coating produced at different concentrations: (a) 0 g/L; (b) 5 g/L; (c) 15 g/L; (d) 30 g/L.

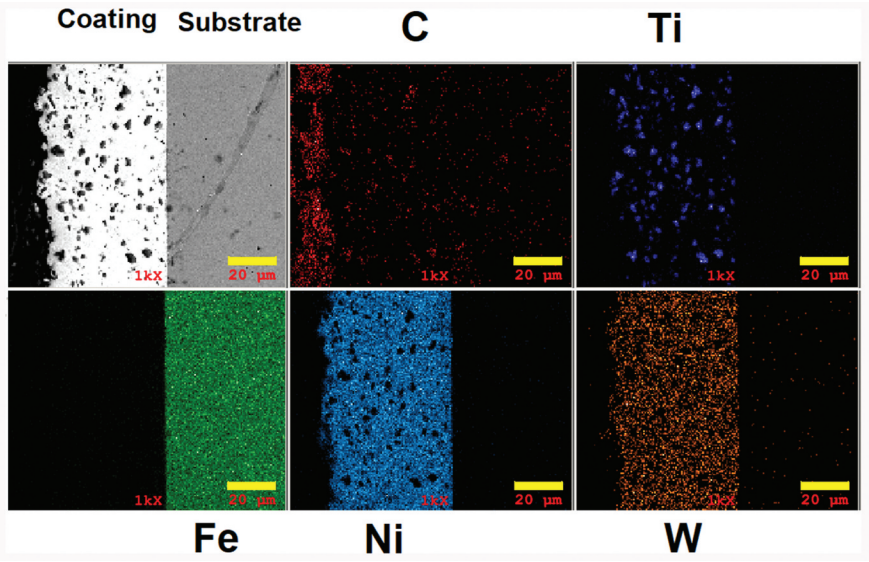

Figure 3. Elemental mapping of cross-sectional of Ni–W–TiC (15 g/L) coating.

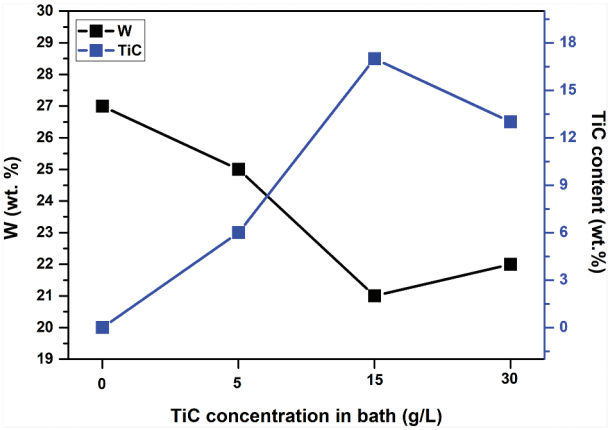

Figure 4. Effect of TiC concentration in the plating bath on the weight percentage of TiC and tungsten in the coating.

decreasing co-deposited TiC particles in the deposited layer. At the same time, the tungsten content decreases in coating slightly with the increase of TiC concentration from 5 to 30 g/L in the solution. The tungsten content obtained from the results of EDX was 25%, 21% and 22 wt% for the coatings deposited at TiC concentrations of 5 g/L, 15 g/L and 30 g/L, respectively. A similar effect was observed by different authors [15,37]. Accordingly, the number of Ni^{2+} adsorbed on particles was low in the electrolyte at a low concentration of particles, resulting in the decreasing amount of co-deposited TiC particles in the matrix. By increasing TiC concentration in the plating bath has generated more amount of suspended particles and contributed further opportunities for particle adsorption onto the coating. However, when the TiC particle concentration increases beyond 15 g/L, the decrease has been observed in the co-deposited particle content and this decreases of TiC particle content which might be due to the concentration saturation causing the particle aggregation emanated from insufficient surfactant concentration. On the other hand, at a TiC concentration of 30 g/L, nickel ions inside the electrolyte could not cover all TiC particles, because of the poor suspension of the TiC particles and this leads to the reduction of the amount of the co-deposited particles. Therefore, in this study, for the studied particle concentration, it is suggested that the TiC particle content in the plating solution should not exceed 15 g/L. These results show that the maximum wt.% of the incorporated particle can be obtained from an electrolyte containing 15 g/L of TiC concentration.

Figure 5a shows the XRD patterns of the coatings obtained at various TiC ceramic particle concentrations in the plating bath. As seen in Figure 5a, three broad peaks exhibited at 2θ angle of ~44°, ~51°, and ~74° which are corresponded to face-centered cubic (FCC)–Ni and predominant crystal planes are (111) (200) and (220) that signifies the formation of a solid solution of tungsten atom in the nickel lattice, which is in agreement with other researches [21,38]. The intensity of the diffraction peaks of the TiC co-–depositions is lower than that of the unreinforced Ni–W deposition. The weak peak at 36.1° is linked to TiC particles incorporated in Ni(W) matrix. As shown in Figure 5b, the TiC peaks possess the maximum intensity at the Ni–W–TiC (15 g/L) composite deposition, compared to the other coatings. Therefore, it is concluded that Ni–W–TiC co-deposition prepared at a concentration of 15 g/L has the maximum TiC content. Moreover, as can be seen in Figure 5c, with an increase in the TiC concentration in the plating bath, the (111) diffraction peak has moved to the left toward lower 2θ angles, which was due to lattice distortion caused by TiC particles. Another reason is larger size W ions were substituted by the smaller size W ions which the decrease in the amount of W at the deposited layer was already given in Figure 4. Compared to the Ni–W alloys, the intensity of the peak

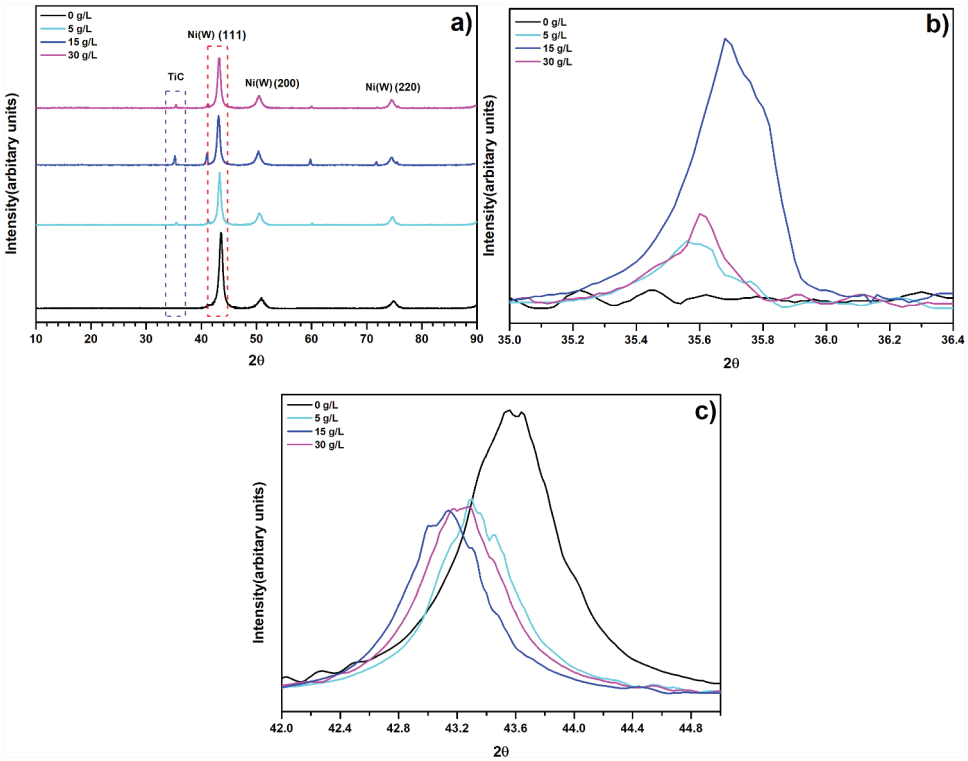

Figure 5. XRD patterns of (a) unreinforced Ni–W and Ni–W–TiC composite deposition; (b) detailed diffraction of TiC; (c) detailed (1 1 1) diffraction of nickel.

of Ni–W–TiC coating became lowering and broadening with the increase of the TiC concentration in the electrolyte. This was attributed to the decreases in the crystallite size of the TiC co-deposition by the addition of TiC particles in the Ni–W coating. According to the FWHM of all peaks of the samples, the crystallite size and microstrain (ε) of all coatings could be calculated according to the Williamson–Hall equation. Williamson–Hall equation as follows [30]:

$$\frac{(\beta\text{size}+\beta\text{strain})\text{Cos}\theta}{\lambda}=\frac{k}{D}+\frac{2\varepsilon\text{Sin}\theta}{\lambda} \quad 2$$

$$\beta_{size}+\beta_{strain}=\beta_{exp}-\beta_{inst} \quad 3$$

Here, k is constant which is 0.9, $\beta_{size}+\beta_{strain}$ denotes the full width at half maximum (FWHM), β_{inst} represents the broadening due to the instrument, λ is the wavelength of CuKa radiation which is 1.54 Å, θ is the Bragg angle, ε is the microstrain and D is the crystallite size.

Figure 6a gives Williamson–Hall plots which were drawn with $2\varepsilon\text{Sin}\theta/\lambda$ along the x-axis and $(\beta_{size}+\beta_{strain})\text{Cos}\theta/\lambda$ along the y-axis for all diffraction peaks of Ni–W alloy and Ni–W–TiC coating. As a result, the slope and y-intersect of the fitted line give strain and crystallite size, respectively. Figure 6b displays that the incorporation of TiC particles has a significant impact on the microstrain and crystallite size of TiC co-deposition. It can be calculated that the crystallite sizes of samples were 10.4, 9.9, 9.22, and 7.68 nm for the coatings deposited at TiC ceramic particle concentrations of 0, 5, 15, and 30 g/L, respectively. Obviously, the crystallite size of Ni–W–TiC coating decreased with the increase

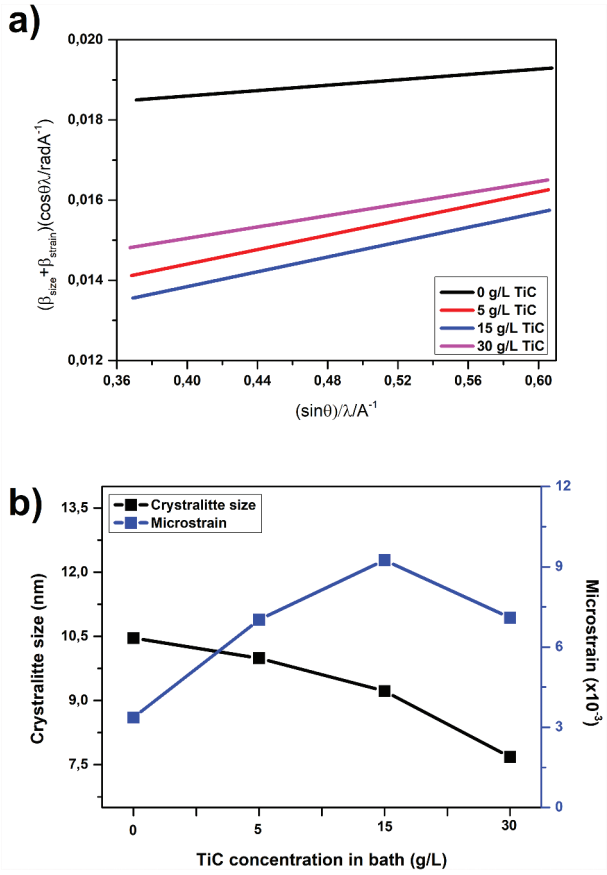

Figure 6. (a) Williamson–Hall plot and (b) Crystallite size and microstrain of the unreinforced Ni–W and Ni–W–TiC composite coating produced with various particle concentrations.

of TiC concentration in the solution from 5 to 15 g/L, then increased with further incorporating TiC from 15 to 30 g/L. As is well known in the literature for the electrodeposition process, the crystallite size is essentially identified by the grain growth rate and nucleation rate [39,40]. This indicates that TiC is adsorbed on the growing crystal and result in the generation of further nucleation sites for the deposition of nickel ions from the plating bath and thus inhibits the growth of metal crystallites which acting as a barrier for crystals growth and resulting in decrease crystallite size of the coating. In addition, the increasing slope visible in the Williamson–Hall plot (Figure 6b) with increasing TiC concentration indicates that the existence of TiC in the coating leads to a degree of microstrain in the Ni(W) matrix. It has been experienced that the microstrain of Ni–W–TiC coating increased with increasing TiC concentration in the solution and obtained the maximum TiC concentration of 15 g/L. This may be attributed to large lattice mismatch stress between the ceramic particles and nickel matrix and compressive microstrain is generated. By increasing the particle concentration to 30 g/L leads to decreasing the microstrain of TiC co-deposition because of particle aggregation.

The mechanical properties, i.e. hardness and elastic modulus, of the Ni–W, and Ni–W–TiC coating produced with various particle concentrations were carried out by the nanoindentation method. The results are exhibited in Figure 7a as a function of TiC particle concentration in the plating bath for coating. The hardness of Ni–W alloy was 7.4 GPa, whereas the elastic modulus was 206 GPa. As it can be seen in Figure 7a, the incorporation of TiC ceramic particles significantly improves the elastic modulus and nano hardness of the coating. Moreover, it can be concluded that the hardness and elastic modulus of coating first increases with the increase of concentrations TiC in the electrolyte then decreased when surpassed 15 g/L. For example, hardness and elastic modulus of the Ni–W–TiC coating deposited with 15 g/L is 8.3 GPa and 207 GPa, respectively, while at 5 g/L, they are 7.8 GPa and 204 GPa, respectively, which means nearly 8% and 1.4% enhancement in the nano hardness and elastic modulus of the Ni–W–TiC coating containing 15 g/L as compared to those of the co-deposited with 5 g/L. Improvement in the hardness of TiC co-deposition might be associated with several mechanisms like grain boundary strengthening (Hall–Petch relationship), and dispersion strengthening (Orowan mechanism) [41,42]. As reported above, the addition of TiC particles into the electrolyte decreases the crystallite size of coating and results in increasing the volume of grain boundaries which inhibited dislocation motion in the matrix; thus, based on Hall–Petch equation, the coating hardness is increased. The second reason for hardness improvement can be due to the Orowan

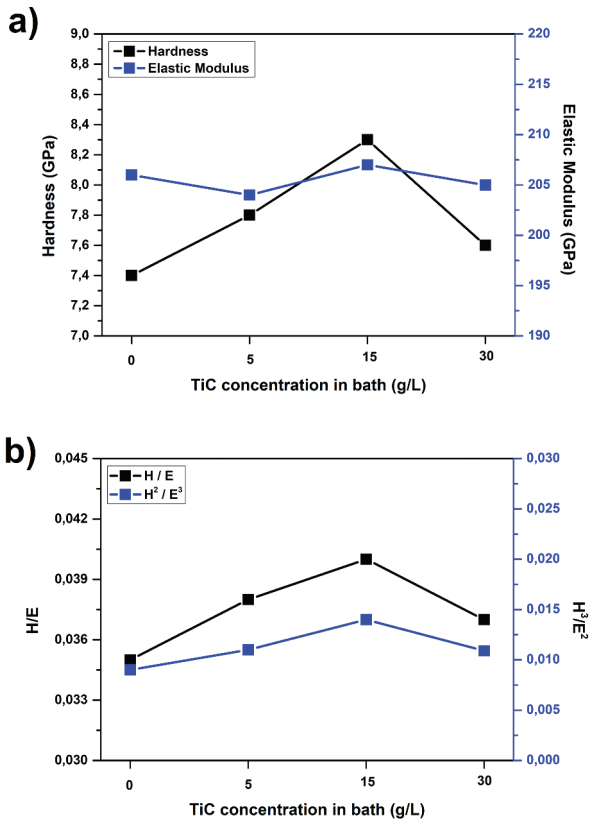

Figure 7. Nanoidentation results as for unreinforced Ni–W and Ni–W–TiC composite coating produced with various particle concentration (a) H/E and (b) H^3/E^2 ratio.

mechanism which is the dispersive strengthening effects of TiC particles. According to the Orowan mechanism, once the distance between the second phase particles decreases, the hardness of the coating is improved. The increasing amount of TiC particles incorporating in the nickel matrix result in the distance between particles decreased. Furthermore, the TiC ceramic particles used as a reinforcement serve as barriers to block dislocation movement in the matrix and grain boundary sliding of the matrix and so impede the plastic deformation of the Ni(W) matrix. On the other hand, ceramic particle–nickel matrix interfaces have significant roles in mechanical properties improvement of the co-deposited of TiC particle. The existence of ceramic particle–nickel matrix interfaces that have excellent stability and limited mobility can strengthen the grain boundaries of the nickel matrix and hinder the plastic deformation of the matrix [43]. Therefore, according to what was mentioned above, improvement of mechanical properties of TiC co-deposition (15 g/L) can be attributed to the formation of an excellent interface between nickel matrix and ceramic particle and the homogeneous distribution of TiC particles in the Ni(W) matrix. Our results are consistent with those reported by Wang et al [44]. However, when the TiC concentration increases to 30 g/L, the hardness and elastic modulus decreased to 7.6 and 205 GPa, respectively. This decrease can be

related to the agglomeration and non–uniform distribution of ceramic particles in the nickel matrix.

Authors have reported that the ratio between the hardness and the elastic modulus is guidance for predicting the tribological behavior of coatings than the hardness itself [45,46]. It has been suggested that high H/E and H^3/E^2 values for coatings are a key point for long service life and application under high contact loads. The ratio between H and E is can be used to predict the mechanical failure of the coating, while the H^3/E^2 ratio related to the plastic deformation resistance factor of the material. Qi has suggested [45] that the most durable coatings can be produced in cases of high elastic strain to failure and this can be performed by achieving coatings high hardness in order to resist plastic deformation and with a low elastic modulus. The H/E and H^3/E^2 ratios of coatings were shown in Figure 7b. As can be seen in Figure 7b, Ni–W–TiC coating deposited at 15 g/L had the highest H/E ratio of ~0.040 and H^3/E^2 ratio of ~0.014 GPa.

Figure 8 shows wear rates and friction coefficients of Ni–W–TiC deposition produced at various TiC contents. In the case of Ni–W, the friction coefficient continuously increases as increasing the sliding distance and shows no stabilization even after 400 m sliding distance yielding a friction coefficient of 0.5. The friction coefficient of all Ni–W–TiC coatings shows almost similar characteristics to the sliding distance. Except for the coating that deposited by busing 30 g/L TiC in the electrolyte, friction coefficients exhibited relatively stable behavior after a sliding distance of 300 m with flattening of asperities because of increasing the contact area. With the increasing TiC particle concentrations in the electrolyte, the friction coefficient (COF) of the samples initially decreases and then increases after the concentration over 15 g/L. As seen from Figure 8a, Ni–W–TiC (30 g/L) coating shows a higher friction coefficient compared with all coatings which can be due to the rough surface of the coating and aggregation of particles. Another reason for the high coefficient of friction may be weak interfacial bonding between the ceramic particles and matrix, which leads to the pulling out of TiC particles during the wear test. However, the Ni–W–TiC (15 g/L) coating with the highest TiC content displayed the lowest coefficient of friction. These results are attributed to, not only the uniform distribution of the TiC ceramic particles in the nickel matrix but also uniform microstructure and high mechanical properties [47].

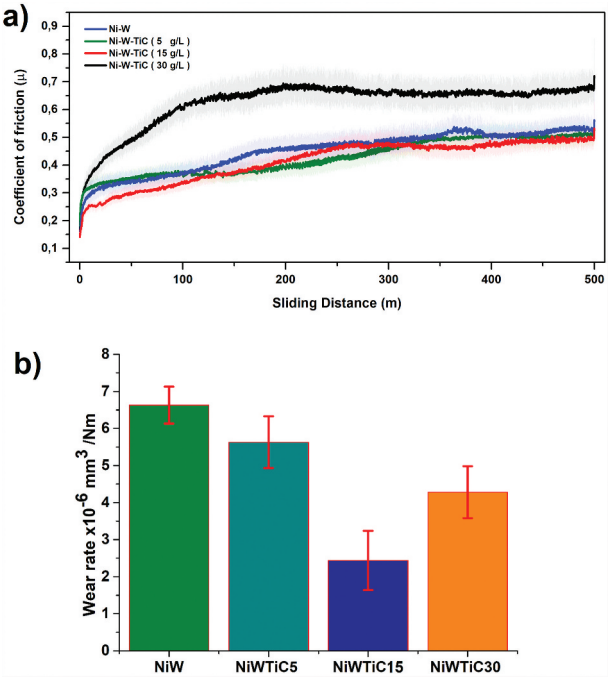

Figure 8. (a) The friction curves and (b) Wear rates of the Ni–W and Ni–W–TiC composite coating produced at different TiC concentrations.

As shown in Figure 8b, the wear rate decreases continuously upon increasing the ceramic particle concentration in the deposition bath and reaches a minimum value at 15 g/L then further increases at 30 g/L. The wear rate was obtained to be 6.6×10^{-6}, $5.6 \times 10^{-6,}$ 2.4×10^{-6}, 4.2×10^{-6} for the coatings produced at current density 10 A/dm^2 and ceramic particles concentration of 0 g/L 5 g/L, 15 g/L, 30 g/L, respectively. This decrease in wear rate can be explained as the increased hardness and toughness with the increased H/E and H^3/E^2 ratios [44]. When the incorporation TiC concentration of 30 g/L, the wear rate increase to 4.25×10^{-6} mm^3 N/m for Ni–W–TiC coating because of the agglomeration of incorporated TiC particles into the matrix which results in increasing the contact surface between the abrasive surface and the coating. It indicates that Ni–W–TiC coatings produced with TiC concentration of 15 g/L deposits in this work shows the best wear resistance. This is attributed to the role of the TiC ceramic particles which improve the strength and hardness of the nickel matrix, according to the Orowan and Hall–Petch mechanisms [48]. Moreover, during sliding wear, TiC ceramic particles decrease the direct contact between the Ni(W) matrix and M50 ball.

Figure 8 shows high magnification SEM images of the worn surface of the co-deposition produced at different TiC concentrations. As indicated in Figure 9, the worn surface of unreinforced Ni–W coating is characterized by heavy plastic deformation and grooves along the sliding direction. These results demonstrate that the dominant wear mechanism is governed by adhesive wear. Because of the plastic deformation hardening for the unreinforced coating, the formation of fatigue cracks and subsequent delamination wear is the most effective phenomenon (Figure 9a) After incorporation TiC particles into the Ni(W) matrix, the worn surface of the Ni–W–TiC (5 g/L) coating shows increasing the crack wideness with a decreased amount of cracks and smoother surfaces compared

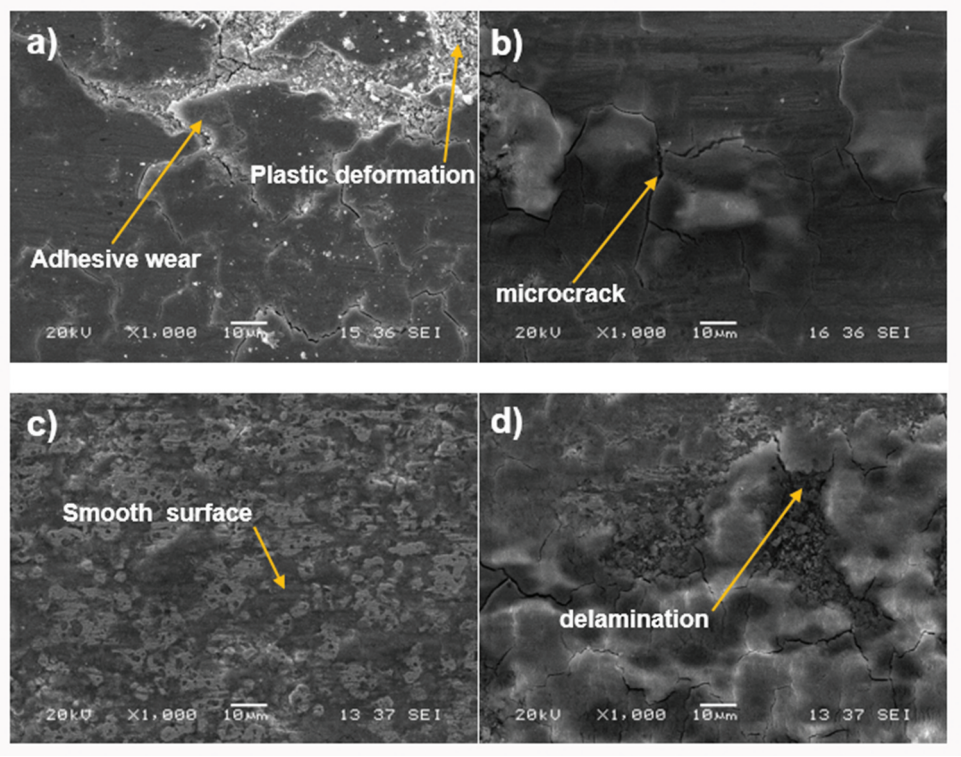

Figure 9. SEM image of the wear tracks of the Ni–W and Ni–W–TiC composite coating produced at different TiC concentrations: (a) 0 g/L; (b) 5 g/L; (c) 15 g/L; (d) 30 g/L.

with that of unreinforced Ni–W coating. There seems no delamination to be started which was attributed contribution of TiC particles for load–bearing in the composite (Figure 9b). However, it is suggested that the surface of TiC co-deposited (5 g/L) coating has potential after plastic deformation and following cracks formation then exhibit delamination wear with increasing sliding distance. The worn surface of the Ni–W–TiC coating produced by 15 g/L particle concentration in the bath has free-crack and relatively smooth because ceramic particles can bear the stresses and reduce the plastic deformation. During the sliding test, friction heat occurring at the interface nickel matrix and ball, the nickel matrix causes to soften of Ni(W) matrix then debris was formed on the worn surface. While the content of TiC particles in the coating increases, the area fractions of debris on the wear track decreases. The dispersion uniformly TiC particles in the Ni(W) matrix has improved the mechanical properties and this obviously can improve the wear resistance by hindering the deformation of the matrix during the sliding process. The excellent wear resistance of Ni–W–TiC (15 g/L) coating can also be attributed to improved surface hardness and high load–bearing capacity of TiC particles with the increase in the amount of reinforcement in the Ni(W) matrix. The increased amount of smooth areas is attributed to the increased load–bearing capacity due to incorporated TiC particles into the matrix. Thus, increasing TiC particles in the Ni(W) matrix leads to an improved wear resistance due to decreasing area fractions of debris. As can be seen from Figure 9c, the formed debris at the surface adheres to the worn surface of Ni–W–TiC coating deposited with 15 g/L. Compared with coatings Ni–W–TiC (5 g/L), the worn surface becomes smooth and the transfer layer is formed around particles as exhibited in Figure 9c. Moreover, this debris was flattened by the M50 steel ball during the sliding test, result in decreasing the roughness of the wear track. The hardness of this kind of transfer layer is high because of the presence of ceramic particles and the work hardening. Moreover, the formation transfer layer reduced the contact between the Ni(W) matrix and counterface ball thus, the wear rate of TiC co-deposition (15 g/L) is diminished. Further increasing TiC particle concentration, the Ni–W–TiC (30 g/L) coating exhibits more wear debris by severe plastic deformation associated with delamination (Figure 9d). Moreover, the worn surface of the coating has occurred with some delaminated cracks. Formed the layer on the worn surface is broken down due to the TiC particles agglomeration and loosely bonded ceramic particles in some regions and is partially removed from the contact, leading to a sharp increase in wear rate and COF.

Figure 10a is shown the open-circuit potential plots for Ni–W coating and Ni–W–TiC co-deposition. It is observed that the incorporating of TiC particles into the matrix significantly firstly increased open–circuit potential toward more positive values which lead to decreasing the formation of galvanic corrosion. Then, further increasing TiC particle concentration decreases open-circuit potential. These results show that

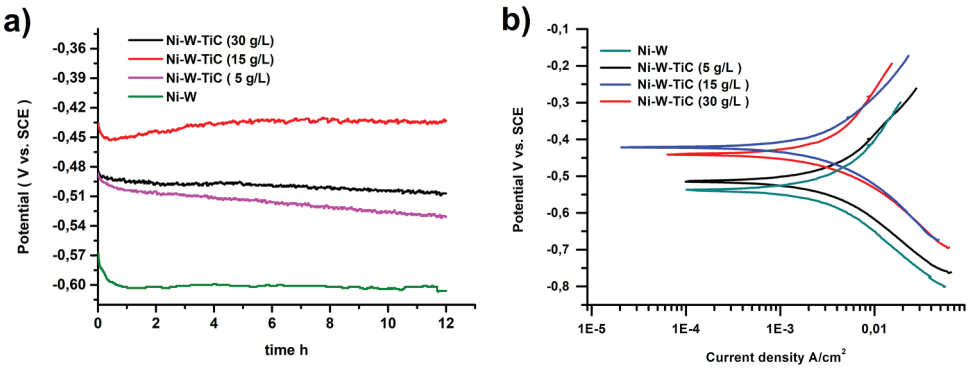

Figure 10. (a) Variation of the open-circuit potential and (b) polarization curves for Ni–W and Ni–W–TiC composite coating in the 3.5% NaCl solution.

a stationary value was observed after about ~1.5 h of the immersion for Ni–W coating produced with a TiC concentration of 15 g/L, indicating displaying excellent chemical stability. The polarization curve of the Ni–W and Ni–W–TiC co-deposition produced with various TiC particle concentrations is shown in Figure 10b. The corrosion resistance of composite deposition is mainly affected by chemical compositions and surface morphology, crystallite size, preferred orientation as well as, interfacial bonding with matrix, amount and uniform distribution of ceramic particles [25,49]. The values of corrosion potential and current density were calculated from the Tafel curve after testing in 3.5 wt% NaCl solution. As can be seen in Tafel curves, at all coatings, passivation not occurred in the curves can be attributed to the formation dissolution reaction in anodic reaction and evolution of the oxygen in the cathodic reaction. As seen in Table 2, unreinforced Ni–W coating exhibits its E_{corr} = −0.53 V and I_{corr} = 4.12 μA cm^{-2}. After incorporating TiC (5 g/L), Ecorr of Ni–W coating has a positive shift of around −0.51 mV compared with unreinforced Ni–W coating. Furthermore, the Ecorr of Ni–W–TiC coating deposited with 15 g/L is −0.41 V, which is more positive than that of unreinforced Ni–W and Ni–W–TiC (5 g/L) coating. The corrosion properties of Ni–W–TiC (30 g/L) coating deteriorate due to agglomerates of particles which easily removed from the surface due to loosely bound to the Ni(W). Ni–W deposition produced with TiC content of 15 g/L shows lower corrosion current density and higher corrosion potential compared to other coatings. The main reasons for the enhancement of corrosion resistance of co-deposition may be attributed to that the reduction in defects such as porosities and voids with the addition of TiC particles which results in hindering corrosive ion diffusion to the Ni(W) matrix [25]. Another reason, the presence of the ceramic particle in Ni(W) matrix not only diminishes the active area prone to corrosion but also refine the grain of the microstructure of coatings, make the coating smooth and uniform. On the other hand, the uniform dispersion of TiC ceramic particles enhances the mechanical properties of the co-deposition and hinder the Ni(W) dissolution [50]. Therefore, for the reasons mentioned above, it is evident that a better corrosion performance was obtained for Ni–W–TiC coating containing 15 g/L in our study.

Figure 11 shows the Nyquist plots for the samples produced via pulse electrodeposition. It is evident from Figure 6 that the curves in the Nyquist of all coatings appear to be similar concerning their shape but they are semicircular arc with different sizes. Moreover, Ni–W and Ni–W–TiC co-deposition show the formation of a single semicircle arc. It has been suggested that a large radius of impedance semicircle for coatings shows improving the corrosion properties of the coatings [51]. Obviously, the radius of the impedance of coatings firstly increased with the increase of TiC particle content in the electrolyte then decreased with further incorporating ceramic

Table 2. Corrosion parameters obtained from the polarization curves for unreinforced Ni–W and Ni–W–TiC coatings.

Coatings	Ecorr vs. SCE (V)	icorr (mA cm^{-2})
Ni–W	−0.53	4.12
Ni–W–TiC (5 g/L)	−0.51	3.71
Ni–W–TiC (15 g/L)	−0.41	2.76
Ni–W–TiC (30 g/L)	−0.44	3.25

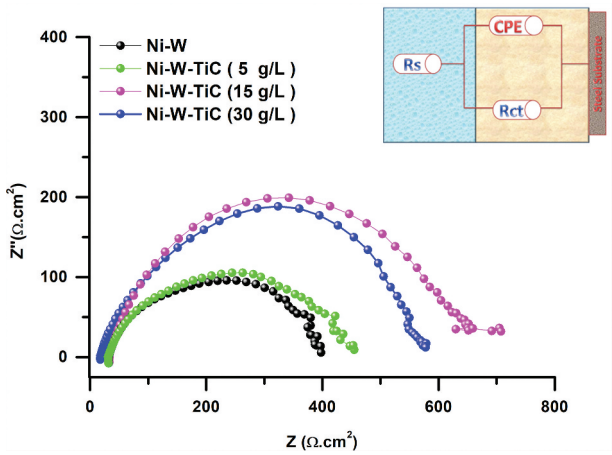

Figure 11. Nyquist plots of the unreinforced Ni–W and Ni–W–TiC co-deposition produced at different TiC concentrations. Inset of the equivalent circuit model.

Table 3. Electrochemical parameters derived from the fitting.

Coating	Rs	Rct	Qdl ($\times 10^{-5}$ F)
Ni–W	5.9	798	15.4
Ni–W–TiC (5 g/L)	6.2	985	14.7
Ni–W–TiC (15 g/L)	9.5	1241	11.3
Ni–W–TiC (30 g/L)	6.5	1085	13.1

particle from 15 to 30 g/L. It is clearly seen that the largest radius of the impedance semicircle was obtained for Ni–W–TiC composite deposition produced at 15 g/L. The equivalent circle consists of R_{CT} R_s C_{PE} which are, electron transfer resistance, electrolyte resistance and constant phase element, respectively. The EIS data of samples by fitting are listed in Table 3. It has been established that high values of R_{ct} and low values of R_s imply benefits to improve corrosion resistance. As seen in Table 3, the R_{ct} value increased with the addition of TiC particles in the coating, while the CPE_{dl} values reduced, thus improving the corrosion resistance of the coating. It can be concluded that TiC particles act as a physical barrier against corrosive media such as H_2O and Cl^- and it can decrease the active area prone to corrosion [52]. On the other hand, the existence of TiC into the Ni(W) matrix hindered the dissolution of the matrix and the diffusion of the corrosive environment, leading to the formation of a more homogenous and dense coating. These results are in good agreement with the results of the Tafel curve obtained.

4. Conclusions

In summary, we successfully produced the Ni–W TiC coatings employing pulse electrodeposition and investigated its tribology, nano hardness, corrosion properties under various TiC concentrations at the solution. The calculation of XRD results obtained that the incorporation of TiC in the Ni (W) matrix would result in the microstrain, which further caused lattice distortion of the Ni(W) matrix due to the presence of TiC. On the other hand, the wear resistance of the coatings is estimated by the H/E and H^3/E^2 ratios. Thus, the wear resistance of the composites is significantly affected by the mechanical properties. Based on the above analysis, the lowest values of wear rate and friction coefficient are obtained at the highest values of H^3/E^2 and H/E ratios. Obviously, the addition of TiC particles in the Ni(W) matrix played an important role in determining the mechanical, tribology, and electrochemical properties of the Ni–W–TiC coating. Corrosion and tribological properties of the coatings were gradually improved with increased TiC concentrations in the bath and the best results were obtained at 15 g/L concentration.

Acknowledgments

This work has been supported by the National Boron Research Institute of Turkey (Grant No: 2017–31–07–25–001)

Disclosure statement

No potential conflict of interest was reported by the authors.

Funding

This work was supported by the National Boron Research Institute of Turkey (Grant No: 2017-31-07-25-001).

ORCID

Hasan Algül http://orcid.org/0000-0002-4348-8865
Hatem Akbulut http://orcid.org/0000-0002-6299-136X

References

[1] Safavi MS, Tanhaei M, Ahmadipour MF, et al. Electrodeposited Ni–Co alloy–particle composite coatings: a comprehensive review. Surf Coatings Technol [Internet]. 2020;382:125153.
[2]. Lelevic A, Walsh FC. Electrodeposition of NiP composite coatings: a review. Surf Coat Technol. 2019; 378.
[3] Karimzadeh A, Aliofkhazraei M, Walsh FC. A review of electrodeposited Ni–Co alloy and composite coatings: microstructure, properties and applications. 463–498. Surf Coat Technol. 2019;372.
[4] Demir M, Kanca E, Karahan İH. Characterization of electrodeposited Ni–Cr/hBN composite coatings. J Alloys Compd. 2020;844.
[5] Ghaziof S, Golozar MA, Raeissi K. Characterization of as–deposited and annealed Cr–C alloy coatings produced from a trivalent chromium bath. J Alloys Compd. 2010;496(1–2):164–168.
[6] Zeng Z, Wang L, Liang A, et al. Tribological and electrochemical behavior of thick Cr–C alloy coatings electrodeposited in trivalent chromium bath as an alternative to conventional Cr coatings. Electrochim Acta. 2006;52(3):1366–1373. .
[7] Wasekar NP, Sundararajan G. Sliding wear behavior of electrodeposited Ni–W alloy and hard chrome coatings. Wear. 2015;342-343:340–348.
[8] Wang L, Gao Y, Xue Q, et al. A novel electrodeposited Ni–P gradient deposit for replacement of conventional hard chromium. Surf Coat Technol. 2006;200 (12–13):3719–3726.
[9] Wang Y, Cao D, Gao W, et al. Microstructure and properties of sol–enhanced Co–P–TiO2 nano–composite coatings. J Alloys Compd. 2019;792:617–625.
[10] Doğan F, Uysal M, Duru E, et al. Pulsed electrodeposition of Ni–B/TiN composites: effect of current density on the structure, mechanical, tribological, and corrosion properties. Journal of Asian Ceramic Societies. 2020;8(4):1271–1284.
[11] Electroless UM. Codeposition of Ni–P composite coatings: effects of graphene and TiO2 on the morphology, corrosion, and tribological properties. Metall Mater Trans A Phys Metall Mater Sci. 2019;50(5):2331–2341.
[12] Indyka P, Beltowska–Lehman E, Tarkowski L, et al. Structure characterization of nanocrystalline Ni–W alloys obtained by electrodeposition. J Alloys Compd. 2014;590:75–79.
[13] Vamsi MVN, Wasekar NP, Sundararajan G. Influence of heat treatment on microstructure and mechanical

properties of pulse electrodeposited Ni–W alloy coatings. Surf Coat Technol. 2017;319: 403–414.
[14] Malay KD, Rongxia L, Jiaqian Q, et al. Effect of electrodeposition conditions on structure and mechanical properties of Ni–W/diamond composite coatings. Surf Coat Technol. 2017;309: 337–343.
[15] Jinlong L, Zhuqing W, Tongxiang L, et al. Effect of tungsten on microstructures of annealed electrodeposited Ni–W alloy and its corrosion resistance. Surf Coat Technol. 2018;337: 516–524.
[16] Denise Y, Christopher JM, Fiona YC, et al. Microstructure and fracture toughness of electrodeposited Ni–21 at.% W alloy thick films. Acta Mater. 2018;143:272–280.
[17] Wasekar NP, Latha SM, Ramakrishna M, et al. Pulsed electrodeposition and mechanical properties of Ni–W/SiC nano–composite coatings. Mater Des. 2016;112:140–150.
[18] Sangeetha S, Kalaignan GP, Anthuvan JT. Pulse electrodeposition of self–lubricating Ni–W/PTFE nanocomposite coatings on mild steel surface. Appl Surf Sci. 2015;359:412–419.
[19] Beltowska–Lehman E, Indyka P, Bigos A, et al. Effect of current density on properties of Ni–W nanocomposite coatings reinforced with zirconia particles. Mater Chem Phys. 2016;173:524–533.
[20] Li B, Li D, Mei T, et al. Fabrication and characterization of boron nitride reinforced Ni–W nanocomposite coating by electrodeposition. J Alloys Compd. 2019;777:1234–1244.
[21] Sangeetha S, Kalaignan GP. Tribological and electrochemical corrosion behavior of Ni–W/BN (hexagonal) nano–composite coatings. Ceram Int. 2015;41 (9):10415–10424.
[22] He T, He Y, Li H, et al. A comparative study of effect of mechanical and ultrasound agitation on the properties of pulse electrodeposited Ni–W/MWCNTs composite coatings. J Alloys Compd. 2018;743:63–72.
[23] Gyawali G, Joshi B, Tripathi K, et al. Preparation of Ni–W–Si3N4composite coatings and evaluation of their scratch resistance properties. Ceram Int. 2016;42 (2):3497–3503. .
[24] Li B, Zhang W, Zhang W, et al. Preparation of Ni–W/SiC nanocomposite coatings by electrochemical deposition. J Alloys Compd. 2017;702:38–50.
[25] Wang Y, Zhou Q, Li K, et al. Preparation of Ni–W–SiO2 nanocomposite coating and evaluation of its hardness and corrosion resistance. Ceram Int. 2015;41(1):79–84.
[26] Goldasteh H, Rastegari S. The influence of pulse plating parameters on structure and properties of Ni–W–TiO2 nanocomposite coatings. Surf Coat Technol. 2014;259: 393–400.
[27] Li B, Zhang W, Mei T, et al. Fabrication of Ni–B/TiC–Y2O3 nanocomposites by one–step electrodeposition at different duty cycle and evaluation of structural, surface and performance as protective coating. J Alloys Compd. 2020;823:153888.
[28] Li B, Zhang W. Facile synthesis and electrochemical properties of a novel Ni–B/TiC composite coating via ultrasonic–assisted electrodeposition. Ultrason Sonochem. 2020;61:104837.
[29] Choi JH, Gyawali G, Dhakal DR, et al. Electrodeposited Ni–W–TiC Composite Coatings: effect of TiC Reinforcement on Microstructural and Tribological Properties. Acta Metall Sin (English Lett). 2020;33 (4):573–582. .
[30] Carpenter CR, Shipway PH, Zhu Y. The influence of CNT co–deposition on electrodeposit grain size and hardness. Surf Coatings Technol [Internet]. 2011;205 (21–22):5059–5063.
[31] Su J, Li Y, Duan MG, et al. Investigation on particle strengthening effect in in–situ TiB2/2024 composite by nanoindentation test. Mater Sci Eng A. 2018;727:29–37.
[32] Uysal M, Akbulut H, Tokur M, et al. Structural and sliding wear properties of Ag/Graphene/WC hybrid nanocomposites produced by electroless co–deposition. J Alloys Compd. 2016;654:185-195.
[33] He Y, Wang SC, Walsh FC, et al. Self–lubricating Ni–P–MoS2 composite coatings. Surf Coat Technol. 2016;307:926–934.
[34] Zhang Q, Qin Z, Luo Q, et al. Microstructure and nanoindentation behavior of Cu composites reinforced with graphene nanoplatelets by electroless co–deposition technique. Sci Rep. 2017;7(1):1–12. .
[35] Bahadormanesh B, Dolati A. The kinetics of Ni–Co/SiC composite coatings electrodeposition. J Alloys Compd. 2010;504(2):514–518.
[36] Alizadeh M, Narouei S. Properties of Ni–Ni3Si composite coatings prepared by electrodeposition and subsequent heat treatment. J Alloys Compd. 2019;772:565–572.
[37] Beltowska–Lehman E, Bigos A, Indyka P, et al. Optimisation of the electrodeposition process of Ni–W/ZrO2 nanocomposites. J Electroanal Chem. 2018;813:39–51.
[38] Allahyarzadeh MH, Aliofkhazraei M, Rezvanian AR, et al. Ni–W electrodeposited coatings: characterization, properties and applications. Surf Coat Technol. 2016;307:978–1010.
[39] Zhang X, Qin J, Das MK, et al. Co–electrodeposition of hard Ni–W/diamond nanocomposite coatings. Sci Rep. 2016;6(1):1–11. .
[40] Wang C, Shen L, Qiu M, et al. Characterizations of Ni–CeO2 nanocomposite coating by interlaced jet electrodeposition. J Alloys Compd. 2017;727:269–277.
[41] Allahyarzadeh MH, Aliofkhazraei M, Rouhaghdam ARS, et al. Electrodeposition of Ni–W–Al2O3 nanocomposite coating with functionally graded microstructure. J Alloys Compd. 2016;666:217–226.
[42] Ghasemi A, Penther D, Kamrani S. Microstructure and nanoindentation analysis of Mg–SiC nanocomposite powders synthesized by mechanical milling. Mater Charact. 2018;142:137–143.
[43] Alizadeh M, Safaei H. Characterization of Ni–Cu matrix, Al2O3 reinforced nano–composite coatings prepared by electrodeposition. Appl Surf Sci. 2018;456:195–203.
[44] Wang L, Zhao Y, Jiang C, et al. Investigation on microstructure and properties of electrodeposited Ni–Ti–CeO2 composite coating. J Alloys Compd. 2018;754:93–104.
[45] Qi S, Li X, Zhang Z, et al. Fabrication and characterisation of electro–brush plated nickel–graphene oxide nano–composite coatings. Thin Solid Films. 2017;644:106–114.
[46] Leyland A, Matthews A. On the significance of the H/E ratio in wear control: a nanocomposite coating approach to optimised tribological behaviour. Wear. 2000;246(1–2):1–11.
[47] Algul H, Tokur M, Ozcan S, et al. The effect of graphene content and sliding speed on the wear mechanism of nickel–graphene nanocomposites. Appl Surf Sci. 2015;359:340–348.

[48] Rupert TJ, Cai W, Schuh CA. Abrasive wear response of nanocrystalline Ni–W alloys across the Hall–Petchbreakdown. Wear. 2013;298-299:120–126.
[49] Singh S, Sribalaji M, Wasekar NP, et al. Microstructural, phase evolution and corrosion properties of silicon carbide reinforced pulse electrodeposited nickel–tungsten composite coatings. Appl Surf Sci. 2016;364:264–272.
[50] He T, He Y, Li H, et al. Fabrication of Ni–W–B4C composite coatings and evaluation of its micro–hardness and corrosion resistance properties. Ceram Int. 2018;44(8):9188–9193. .
[51] Fan Y, He Y, Luo P, et al. Pulse Current Electrodeposition and Characterization of Ni–W–MWCNTs Nanocomposite Coatings. J Electrochem Soc. 2015;162(7):D270–D274. .
[52] Fan Y, He Y, Luo P, et al. Pulse Current Electrodeposition and Properties of Ni–W–GO Composite Coatings. J Electrochem Soc. 2016;163(3):D68–D73. .